Realization of an Ideal Cairo Tessellation in Nickel Diazenide NiN_2: High-Pressure Route to Pentagonal 2D Materials

Maxim Bykov[1,2,*], Elena Bykova[1], Alena V. Ponomareva[3], Ferenc Tasnádi[4], Stella Chariton[5], Vitali B. Prakapenka[5], Konstantin Glazyrin[6], Jesse S. Smith[7], Mohammad F. Mahmood,[1] Igor A. Abrikosov[4], Alexander F. Goncharov[2]

[1] College of Arts and Science, Howard University, Washington, DC 20059, USA

[2] The Earth and Planets Laboratory, Carnegie Institution for Science, Washington, DC 20015, USA

[3] Materials Modeling and Development Laboratory, National University of Science and Technology 'MISIS', 119049 Moscow, Russia

[4] Department of Physics, Chemistry and Biology (IFM), Linköping University, SE-58183 Linköping, Sweden

[5] Center for Advanced Radiation Sources, University of Chicago, 60637 Chicago, Illinois, USA

[6] Photon Sciences, Deutsches Electronen Synchrotron (DESY), D-22607 Hamburg, Germany

[7] HPCAT, X-ray Science Division, Argonne National Laboratory, Argonne, IL 60439, USA

ABSTRACT: Most of the studied two-dimensional (2D) materials are based on highly symmetric hexagonal structural motifs. In contrast, lower-symmetry structures may have exciting anisotropic properties leading to various applications in nanoelectronics. In this work we report the synthesis of nickel diazenide NiN_2 which possesses atomic-thick layers comprised of Ni_2N_3 pentagons forming Cairo-type tessellation. The layers of NiN_2 are weakly bonded with the calculated exfoliation energy of 0.72 J/m^2 which is just slightly larger than that of graphene. The compound crystallizes in the space group of the ideal Cairo tiling (*P*4/*mbm*) and possesses significant anisotropy of elastic properties. The single-layer NiN_2 is a direct bandgap semiconductor, while the bulk material is metallic. This indicates the promise of NiN_2 to be a precursor of a pentagonal 2D material with a tunable direct bandgap.

KEYWORDS: pentagonal 2D materials, nitrides, diazenides, high pressure, penta-graphene

Introduction

Most of the well-known two-dimensional materials like graphene, *h*-BN or transition metal dichalcogenides are based on the hexagonal building blocks.[1,2] The high-symmetry hexagonal tessellation is very natural as the 2D plane can be easily covered by ideal hexagons. The realization of motifs of other symmetries may lead to a plethora of interesting properties like the anisotropic response to external stimulations in black phosphorus.[3] Therefore, the search for basic and simple topologies is especially important for the design of 2D materials. Pentagons are much less common building blocks of 2D materials because regular pentagons cannot tile the surface in a gapless way. Therefore, pentagonal tiling requires pentagons to be distorted.[4] One of the most well-known pentagonal tilings is a Cairo-type tiling (**tts-d** topology, Fig. 1). [5] Recently Zhang *et al*. predicted a carbon allotrope penta-graphene, which consists of out-of-plane distorted C_5 rings, connected together in a pattern resembling Cairo pentagonal tessellation.[6] The distorted pentagonal tiling was also experimentally realized in layered $PdSe_2$, which showed excellent air stability, tunable bandgap and high carrier mobilities.[7]

The sp^3-hybridized carbon atoms in penta-graphene and the buckling of layers in $PdSe_2$ break the π-conjugation and lead to an indirect band gap in these 2D materials.[6,8,9] Shao *et al*. suggested that undistorted AB_2 layers retaining π-conjugation may possess a long-desired intrinsic direct band gap in pentagonal 2D materials.[8] Theoretical studies uncovered a series of pentagonal materials AB_2 (A = Pd, Pt, Ni, Sn, B, Al, Sn; B = S, P, N). [8,10–14] For example, predicted single-layer SnX_2 (X=S, Se, or Te) with pentagonal structure are topological insulators with non-trivial band gaps and promising room temperature applications.[14] Some pentagonal materials are predicted to be excellent catalysts for water splitting.[15,16] However, despite very intensive computational studies, there are still no experimental structures where the pentagonal AB_2 layers are not distorted.

The geometry of an ideal Cairo tiling requires the angles of pentagons to be 3×120° and 2×90°, and each pentagon should have four longer edges and one shorter edge. Two distinct vertices of such a pentagon must be 4 and 3 coordinated. The ratio between the long and the short edge in an ideal Cairo tiling is 1: $(\sqrt{3}-1)$ or 1: 0.732 (Fig. 1). The ratio between 4- and 3-coordinated vertices is 1:2, defining the AB_2 stoichiometry.

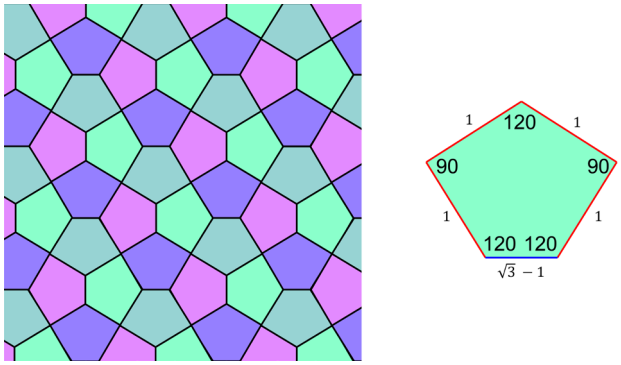

Figure 1. Pentagonal Cairo tiling with ideal geometry.

These geometrical restrictions significantly limit the number of possible candidate structures and allow the design of the compounds to be based on basic chemical and crystal-chemical considerations. A compound must be comprised of two elements in 1:2 ratio with one element having a square-planar coordination and the second element having a planar triangular coordination. The logical choice for the realization of square coordination is one of the group 10 metals (Ni, Pd, Pt), which form very stable 16-electron square-planar complexes. The planar triangular coordination of the second element and the requirement for this element to form short homopolar bonds limits the candidates to B, C, N. Therefore, compounds like MB_2, MC_2 or MN_2 (M = Ni, Pd, Pt) are the logical compounds for the realization of pentagonal Cairo tiling. The consideration of bond length ratio excludes borides as potential candidates: sp^2-hybridized boron connected to two metal atoms and to one boron atom, would have single B-B bonds with a typical length of ~1.8 Å. Therefore, the expected M-B length should be around 2.5 Å, which is significantly larger than any typical M-B bond. Despite the significant number of acetylides of alkaline earth and early transition metals (MC_2)[17] no such compounds are available for the group 10 metals with only interstitial carbides known for Ni (Ni_3C, $Ni_{0.98}C_{0.02}$). [18,19]

Dinitrides of group 10- and many other metals are available at high-pressure conditions.[20–27] Pyrite-structured Pt and Pd pernitrides PtN_2 and PdN_2 were synthesised in laser-heated diamond anvil cells *via* direct reactions between elements at pressures above 48 and 58 GPa respectively.[28,29] Recently marcasite-type NiN_2 was reported by Niwa *et al*. at ~36 GPa.[30] Both pyrite and marcasite-type structures are built of MN_6 octahedra interconnected with each other by sharing common edges or vertices and through strong N-N bonds. Furthermore, both structure types contain hidden Cairo-type tessellation and can be considered as possible precursors to 2D pentagonal materials.[4] While metal pernitrides have been extensively studied at high pressure conditions, their properties at ambient conditions have been examined to a much lesser extent because many of them are not thermodynamically stable. Nevertheless, it is expected that such dinitrides would follow a standard pressure-coordination rule: the coordination number increases at high pressure and decreases on decompression. Therefore, sixfold coordinated metals in high-pressure dinitrides may transform to fourfold coordinated upon decompression, like in the recent example of BeN_4. [31] It was reported before that pyrite-PtN_2 is metastable at ambient conditions, while pyrite-PdN_2 decomposes to elements below 13 GPa.[28,29,32] The structure of ambient-pressure NiN_2 is hitherto unknown.[30] Here we demonstrate the synthesis of nickel diazenide NiN_2 with atomic-thick layers consisting only of Ni_2N_3 5-membered rings and having an ideal space group for the Cairo pentagonal tiling *P*4/*mbm*. This compound represents a long-sought prototype of pentagonal atomic-thick 2D materials.

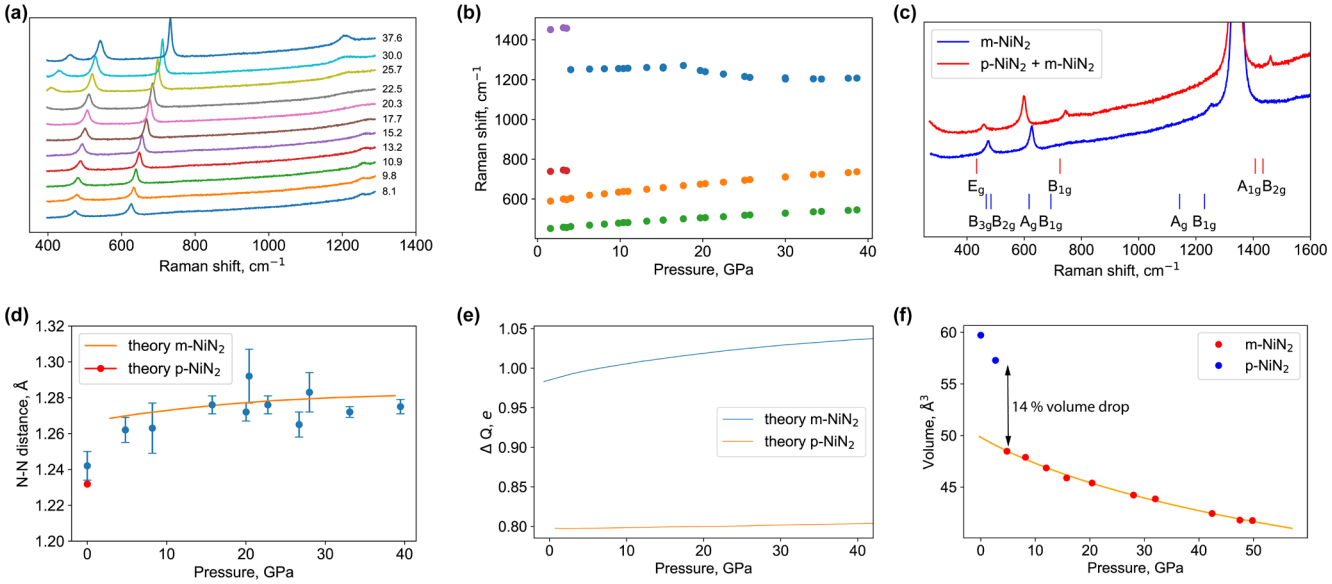

Figure 2. (a) Raman spectra of *m*-NiN_2 at various pressures (b) Raman shifts of Raman-active modes of NiN_2 as a function of pressure (c) Comparison of Raman spectra of *m*-NiN_2 (10.4 GPa) and a mixture of m-NiN_2 and *p*-NiN_2 (3.1 GPa). Red and blue ticks show the positions of calculated Raman-active modes of *p*- and *m*-NiN_2, respectively. (d) Experimental and theoretically predicted N-N distances in *m*-NiN_2 and in *p*-NiN_2 phases. (e) Calculated Bader charge transfer from the Ni atom ΔQ in *m*- and *p*-NiN_2 as a function of pressure (f) Pressure dependence of the unit cell volume of NiN_2. Orange line shows the 3rd order Birch-Murnaghan equation of state (V_0 = 49.8(4) Å^3, K_0 = 165(6) GPa, K' = 5.9(3)).

Results and discussion

High-pressure reactions between nickel and nitrogen at pressures of 37.6, 38.7 and 49.8 GPa (Fig. S1, Table S1) lead to a marcasite-type NiN_2 (*m*-NiN_2) as evidenced by single-crystal X-ray diffraction analysis and agrees with the previous studies of Niwa *et al*.[30] Full experimental and crystallographic details are provided in the Tables S2-S3 and in the supplementary *cif* files. All samples were gradually decompressed down to ambient pressure. Sample #1 was studied by means of single-crystal X-ray diffraction at every pressure step. Samples #2 and #3 were first examined by powder XRD to confirm the synthesis of *m*-NiN_2 and further studied by means of Raman spectroscopy (Fig. 2a-c). Pressure dependence of lattice parameters and unit cell volume between 50 and 4 GPa does not exhibit any peculiarities and is consistent with ref. [30] (Fig. 2f). However, between 4.0 and 3.1 GPa *m*-NiN_2 transforms to a phase with a different structure, which is hereafter referred to as *p*-NiN_2 (*p* stands for "pentagonal" as explained below). *p*-NiN_2 crystallizes in the tetragonal space group *P*4/*mbm* (a = 4.5755(12), c = 2.853(11) Å at ambient conditions) with Ni atoms occupying the Wyckoff site 2*a* (0,0,0) and N atoms occupying site 4*g* (-0.0960(6), 0.4040(6), 0). The structure consists of atomic-thick layers built of Ni_2N_3 pentagons (Fig. 3 a,b). Ni atoms have square-planar coordination to four nitrogen atoms, while each N atom has a planar triangular coordination to two Ni and one N atoms. Trigonal planar coordination of N atoms suggests their sp^2 hybridization and double character of the covalent N=N bond. The double character of the N=N bond is also in agreement with the refined interatomic distance of 1.242(8) Å characteristic for metal diazenides $M^{2+}[N_2]^{2-}$ (M = Ca, Sr, Ba).[33] NiN_2 can be considered as a square planar 16-electron complex, which is typical for group 10 metals. The *m*-NiN_2 → *p*-NiN_2 transformation is characterized by a pronounced volume increase of ~14 % (Fig. 2f), which is related to the change of Ni coordination number.

Interestingly, the N-N distance in *m*-NiN_2 decreases with decreasing pressure as evidenced by the increase of N-N stretching vibration frequencies from 1207 cm^{-1} at 39 GPa to 1250 cm^{-1} at 4 GPa (Fig. 2 a, b). This is also supported by the results of single-crystal structure refinement and theoretical calculations (Fig. 2d). Such unusual and counterintuitive behavior can be explained by the changing of the charge transfer between Ni and $[N_2]$ units upon compression. The N-N distance in a $[N_2]^{x-}$ dimer is extremely sensitive to the charge on this unit. Therefore, the compression of *m*-NiN_2 leads to the increase of the oxidation state of Ni as evidenced by the calculated Bader charge transfer from Ni atoms (Fig. 2e). Moreover, this behavior agrees with the calculated decrease of electronegativity of Ni relative to N at high pressure, which leads to a more ionic character of Ni-N compounds as the pressure rises.[34] We should note the peculiarity in the behavior of the Raman peak at ~1200 cm^{-1} in the pressure range between ~18 and 25 GPa, where it is smeared out and its maximum is shifted to lower wavenumbers (Fig. S2). This may manifest an isostructural transition in this pressure range. *m*-NiN_2 also shows slight changes in compressional behavior of lattice parameters in the same pressure range.[30]

The bulk modulus of *m*-NiN_2 is reported to be 174(5) GPa, which is lower than typical bulk moduli of dinitrides with metals in the oxidation state +3 (*e.g.* FeN_2,[35] RhN_2 [21]), but also much larger than those of diazenides like BaN_2[36]or CuN_2.[27] Upon *m*-NiN_2 → *p*-NiN_2 transformation the frequency of the A_{1g} mode (N-N stretching vibration) discontinuously jumps by ~200 cm^{-1}, which manifests the significant decrease of the N-N bond length and therefore, the partial reduction of Ni along the way from Ni^{3+} to Ni^{2+} in *p*-NiN_2 and also agrees with calculated Bader charges (Fig. 2e). A similar effect is reproduced in calculated phonon dispersions (compare Fig. 4a and Fig. S3) where the shift of the highest frequency optical phonon branch to higher frequencies between *m*-NiN_2 and *p*-NiN_2 is apparent. Note that according to our calculations both phases are dynamically stable at pressure of interest for this study. The *m*-NiN_2 → *p*-NiN_2 transition is also supported by calculations, showing that *p*-NiN_2 becomes lower in enthalpy than *m*-NiN_2 below 7.5 GPa (Fig. S4).

Niwa *et al*. previously observed the transformation of *m*-NiN_2 to a tetragonal structure with a = 3.2111(2) and c = 2.7780(4) Å.[30] The reported lattice parameter c agrees with our finding, but the parameter a differs by a factor of $\sqrt{2}$. Apparently, earlier studies detected only the Ni sublattice because the atomic scattering factor of nitrogen is significantly lower than that of Ni and it might be challenging to observe weak reflections, which are defined by the scattering of only N atoms based solely on the powder XRD (Fig. S5-S6).

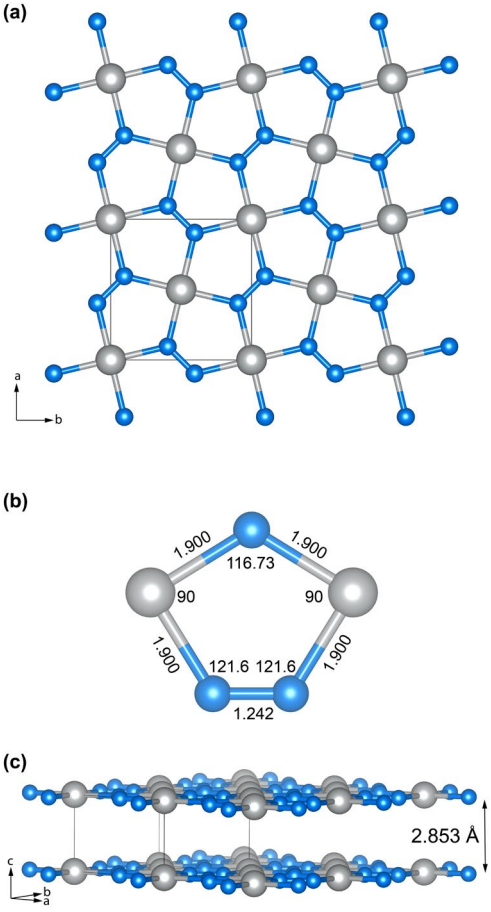

Figure 3. Crystal structure of *p*-NiN_2 at ambient conditions. Blue and grey balls show the positions of N and Ni atoms, respectively. (a) Projection along the c-axis. (b) Geometry of a single Ni_2N_3 pentagon. Numbers indicate interatomic distances (Å) and bond angles (°). (c) Projection showing layer-stacking in *p*-NiN_2.

The layers of *p*-NiN_2 are the example of the simplest non-distorted pentagonal Cairo tiling (**tts-d**). All other known occurrences of **tts-d** topology are either complex metal organic frameworks or severely distorted inorganic structures like $PdSe_2$ [7] or $K_2Sb(P_2O_7)F$. [37]

An interlayer distance of 2.853(11) Å in *p*-NiN_2 at ambient pressure is substantially larger than the Ni-Ni distance in Ni metal (2.47 Å), while the N-N interlayer distance is typical for layered nitrides.[38] Therefore, we can expect that NiN_2 is a layered compound with only weak interactions contribution to the interlayer bonding and significant anisotropy of physical properties and easy cleavage of pentagonal NiN_2 layers. The depletion of the interlayer charge density in *p*-NiN_2 compared to *m*-NiN_2 can be clearly seen on the calculated charge density maps (Fig. S7) and supports interlayer Ni-N bond breaking.

In order to get an insight into the properties of *p*-NiN_2 we have performed theoretical calculations in the framework of density functional theory. The calculated elastic tensor (Table 1) reveals significant anisotropy of the elastic properties of *p*-NiN_2 (Fig. 4b). Young's modulus of *p*-NiN_2 varies between ~42.5 and 658 GPa, which is less anisotropic than graphite or *h*-BN,[39,40] but more anisotropic than most of the transition metal dichalcogenides[41] or MAX phases.[42]

Table 1. Calculated elastic constants C_{ij} (GPa) and maximum and minimum values of Young's modulus *E* (GPa) of *p*-NiN_2.

C_{11}	C_{33}	C_{44}	C_{66}	C_{12}	C_{13}	E_{max}	E_{min}
715.3	83.4	12.7	249.1	200.8	1.5	658.9	42.6

Calculated phonon dispersions (Fig. 4a), besides the demonstration of the dynamic stability of *p*-NiN_2 at ambient pressure *via* the absence of imaginary frequencies, clearly underline the layered nature of the compound and the high elastic anisotropy. This can be immediately recognized by the presence of layer bending modes with quadratic dispersion (Γ → M, Γ→ X paths on the Fig. 4a).[43] We calculated the exfoliation energy (the energy required to remove one atomic layer from the surface of the bulk material) as the difference in the ground-state energy between a slab of N atomic layers and a slab of (N -1) atomic layers plus an atomic layer separated from the slab:

$$E_{exf} = -[E_{N-layer\ slab} - E_{(N-1)-layer\ slab} - E_{single\ layer}],$$

The calculation with $N = 16$ results in $E_{exf} = 0.72$ J/m^2, which is higher than the experimental values in graphene 0.37-0.44 J/m^2,[44] but is of the same order of magnitude, indicating that the NiN_2 monolayer could be prepared experimentally from its bulk form.

Single-layered MN_2 (PtN_2, PdN_2, NiN_2, AlN_2, BN_2) compounds have been addressed in a number of recent publications, where their properties were investigated by means of theoretical calculations.[10–12,45,46] According to Yuan *et al.* [10] the hypothetical single layer of *p*-NiN_2 is thermodynamically, mechanically and dynamically stable. Moreover, the single-layer NiN_2 is predicted to be a direct-bandgap semiconductor (Fig. S8 and Ref. [10]) , while our calculations predict that bulk *p*-NiN_2 is a metal with well-defined pseudogap in a vicinity of the Fermi energy (Fig. 4c, Fig. S9-S10).

In bulk *p*-NiN_2 the density of states (DOS) at the Fermi level is small and arise from the mixture of N-p_z and Ni-d_{z2} orbitals (Fig. S9). The disappearance of the interaction between the layers in a single-layer material leads to a decrease in the DOS at the Fermi level and convert the atomic monolayer to a semiconducting state in agreement with Ref. [10] (Fig. S10). Single-layer *p*-NiN_2 has a significant advantage over predicted penta-graphene and experimentally realized $PdSe_2$ due to the direct band gap, which is achieved through the high-symmetry undistorted atomic-thick layers of NiN_2. Once the layers distort in an out-of-plane manner, a direct-to-indirect bandgap transition occurs. Therefore, the balance between lengths of Ni-N and N-N bonds, which allows the formation of the undistorted pentagonal Cairo-type structure is essential for the electronic properties of *p*-NiN_2.

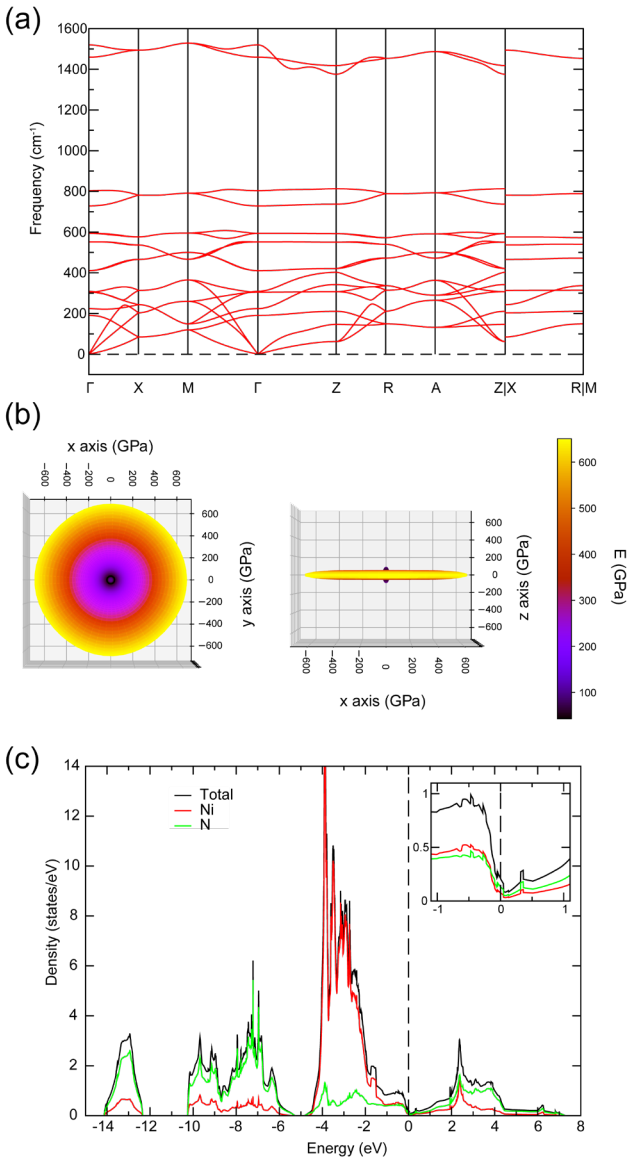

Figure 4. Calculated phonon dispersion relations (a), directional dependence of Young's modulus *E* (b) and electronic density of states plotted relative to the Fermi energy (c) of *p*-NiN_2 at 0 GPa. x,y,z axes in (b) correspond to crystallographic directions [100], [010] and [001] respectively.

Conclusion

In conclusion, here by a combination of crystal chemical design and high-pressure synthesis we have discovered a compound *p*-NiN_2 possessing atomic-thick layers featuring pentagonal Cairo tessellation. The material is recoverable at ambient conditions and is a potential precursor for a pentagonal 2D material with a tunable direct band gap.

Methods

High-pressure synthesis

In every synthesis experiment Ni powder was placed inside a sample chamber of the BX90 diamond anvil cell (DAC) equipped either with Boehler-Almax type diamonds or with standard-cut diamonds with 200-300 μm culet size (Fig. S1). The DACs were loaded with nitrogen gas, which served as a reagent and as a pressure-transmitting medium. The samples were compressed to target pressures (Table 1) and laser-heated at the beamlines P02.2 (PetraIII, DESY, Germany) and GSECARS (APS, USA). In the diffraction experiments pressure was determined using the equation of state of Ni (V_0 = 6.579 cm^3/mol, K_0 = 201 GPa, K' = 4.4).[47] In Raman experiments pressure was determined by the ruby fluorescence.[48]

Synchrotron X-ray diffraction

The high-pressure reaction product contained multiple good-quality single-crystalline domains of NiN_2 and they were characterized by synchrotron single-crystal X-ray diffraction at the beamlines P02.2 (PetraIII, DESY, Germany) and 16IDB (HPCAT, APS, Argonne, USA). At Petra III we used monochromatic X-ray radiation with λ = 0.2908 Å focused by Kirkpatrick-Baez mirror system to ~2×2 $μm^2$ (full width at half maximum). Diffracted intensities were collected by a Perkin Elmer XRD1621 detector. At the beamline 16IDB we used monochromatic X-ray radiation with λ = 0.34453 Å and beam size of ~5×5 $μm^2$. Diffraction images were measured by a Pilatus 1M pixel detector. For the single-crystal XRD measurements samples were rotated around a vertical ω-axis in a range ±30° with an angular step Δω = 0.5° and an exposure time of 1-2 s/frame. For analysis of the single-crystal diffraction data we used the CrysAlisPro software package. Powder diffraction measurements were performed without sample rotation (still images). DIOPTAS software was used to integrate diffraction images to powder patterns. [49] Le-Bail fits of the diffraction patterns were performed with the Jana2006 software. The structure was solved with the ShelXT structure solution program[50] and refined with the Jana2006 and Olex2 programs.[51,52] CSD 2075933-2075937 contain the supplementary crystallographic data for this paper. These data can be obtained free of charge from FIZ Karlsruhe *via* www.ccdc.cam.ac.uk/structures.

Raman spectroscopy

Raman spectra of the samples were collected at GSECARS (APS, Argonne, USA) Raman system with the excitation wavelength of 532.14 nm. Technical details of the system are described elsewhere.[53]

Calculations

DFT calculations were carried out using the projector-augmented-wave (PAW) method[54] as implemented in the Vienna *ab initio* simulation Package.[55–57] For the description of structural, vibrational and mechanical properties, the exchange and correlation energy was described by optB88b-vdW [58] method with nonlocal contributions. This allows us to account for van der Waals interactions. The exchange functional is optimized for the correlation part.[58] The phonon calculations have been performed within the quasiharmonic approximation at temperature T = 0 K using the finite displacement approach implemented into PHONOPY software.[59] A (4×4×6) sized supercell (576 atoms) with 3×3×3 k-point grids has resulted converged phonons for both structures. Bader charge analysis [60] derived from topological consideration on the charge distribution was performed using the code developed by Henkelman *et al.* [61] for 300×300×300 NG(X,Y,Z)F mesh. The elastic constants were calculated from energy-strain relationships with ±1,2% strain and utilized in deriving the directional variation of the Youngs modulus. [62] The factor group analysis approach has been utilized for space group 58 (*m*-NiN_2) and 127 (*p*-NiN_2) to obtain the Raman active irreducible representations, which have been compared with the symmetry of the vibrational modes calculated at Gamma point.

For accurate calculations of the electronic band structure and the electronic density of states, we additionally used the Heyd-Scuseria-Ernzerhof (HSE06) functional with nonlocal screened Coulomb interactions.[63,64] In the HSE06 functional 75% of exchange functional by Perdew *et al*. [65] (PBE) is mixed with 25% Hartree-Fock exchange, while 100% of correlation effects are included in the PBE form. At each volume, the structure was fully optimized (atomic positions and cell shape) until the residual forces on each atom were smaller than 10^{-4} eV/Å. The convergence criterion for the electronic subsystem was chosen as 10^{-5} eV for two subsequent iterations.

The sampling for Brillouin zone integrations is performed using the Gamma scheme with 12×12×22 (*p*-NiN_2) and 12×14×22 (m-NiN_2) k-point grids for optB88b-vdW. In the HSE06 calculations a sampling of 8×8×14 (*p*-NiN_2) and 8×10×14 (*m*-NiN_2) were employed. The energy cut-off for the plane waves was set to 700 eV.

ASSOCIATED CONTENT

Supporting Information. Crystallographic tables, powder diffraction pattern, calculated density of states, band structure, phonon dispersion curves, charge density maps of p-NiN_2 and m-NiN_2. This material is available free of charge *via* the Internet at http://pubs.acs.org." CSD 2075933-2075937 contain the supplementary crystallographic data for this paper. These data can be obtained free of charge from FIZ Karlsruhe *via* www.ccdc.cam.ac.uk/structures.

Corresponding Author

* maks.byk@gmail.com

The authors declare no competing financial interest.

Funding Sources

Research was sponsored by the Army Research Office and was accomplished under the Cooperative Agreement Number W911NF-19-2-0172. Theoretical analysis of chemical bonding was supported by the Russian Science Foundation (Project No. 18-12-00492). Calculations of the phonon dispersion relations were supported by the Ministry of Science and Higher Education of the Russian Federation in the framework of Increase Competitiveness Program of NUST MISIS (No. K2-2020-026) implemented by a governmental decree dated 16 March 2013, No. 211. Support from the Knut and Alice Wallenberg Foundation (Wallenberg Scholar Grant No. KAW-2018.0194), the Swedish Government Strategic Research Areas in Materials Science on Functional Materials at Linköping University (Faculty Grant SFO-Mat-LiU No. 2009 00971) and SeRC, the Swedish Research Council (VR) grant No. 2019-05600 and the Vinnova VINN Excellence Center Functional Nanoscale Materials (FunMat-2) Grant 2016–05156 is gratefully acknowledged. The computations were enabled by resources provided by the Swedish National Infrastructure for Computing (SNIC) partially funded by the Swedish Research Council through

grant agreement no. 2016-07213. GeoSoilEnviroCARS is supported by the National Science Foundation – Earth Sciences (EAR – 1634415) and Department of Energy-Geosciences (DE-FG02-94ER14466). HPCAT operations are supported by DOE-NNSA's Office of Experimental Sciences. Advanced Photon Source is U.S. Department of Energy (DOE) Office of Science User Facility operated for the DOE Office of Science by Argonne National Laboratory under Contract No. DE-AC02-06CH11357.

ACKNOWLEDGMENT

Parts of this research were carried out at the Extreme Conditions Beamline (P02.2) at DESY, a member of Helmholtz Association (HGF). Portions of this work were performed at GeoSoilEnviroCARS (The University of Chicago, Sector 13) and at HPCAT (sector 16) of the Advanced Photon Source (APS), Argonne National Laboratory.

REFERENCES

(1) Novoselov, K. S.; Jiang, D.; Schedin, F.; Booth, T. J.; Khotkevich, V. V.; Morozov, S. V.; Geim, A. K. Two-Dimensional Atomic Crystals. *Proc. Natl. Acad. Sci.* **2005**, *102*, 10451–10453.

(2) Novoselov, K. S.; Geim, A. K.; Morozov, S. V.; Jiang, Y.; Dubonos, S. V.; Grigorieva, I. V.; Firsov, A. A. Electric Field Effect in Atomically Thin Carbon Films. *Science.* **2004**, *306*, 666–669.

(3) Xia, F.; Wang, H.; Jia, Y. Rediscovering Black Phosphorus as an Anisotropic Layered Material for Optoelectronics and Electronics. *Nat. Commun.* **2014**, *5*, 4458.

(4) Zhuang, H. L. From Pentagonal Geometries to Two-Dimensional Materials. *Comput. Mater. Sci.* **2019**, *159*, 448–453.

(5) O'Keeffe, M.; Peskov, M. A.; Ramsden, S. J.; Yaghi, O. M. The Reticular Chemistry Structure Resource (RCSR) Database of, and Symbols for, Crystal Nets. *Acc. Chem. Res.* **2008**, *41*, 1782–1789.

(6) Zhang, S.; Zhou, J.; Wang, Q.; Chen, X.; Kawazoe, Y.; Jena, P. Penta-Graphene: A New Carbon Allotrope. *Proc. Natl. Acad. Sci. U. S. A.* **2015**, *112*, 2372–2377.

(7) Oyedele, A. D.; Yang, S.; Liang, L.; Puretzky, A. A.; Wang, K.; Zhang, J.; Yu, P.; Pudasaini, P. R.; Ghosh, A. W.; Liu, Z.; Rouleau, C. M.; Sumpter, B. G.; Chisholm, M. F.; Zhou, W.; Rack, P. D.; Geohegan, D. B.; Xiao, K. PdSe2: Pentagonal Two-Dimensional Layers with High Air Stability for Electronics. *J. Am. Chem. Soc.* **2017**, *139*, 14090–14097.

(8) Shao, X.; Liu, X.; Zhao, X.; Wang, J.; Zhang, X.; Zhao, M. Electronic Properties of a π-Conjugated Cairo Pentagonal Lattice: Direct Band Gap, Ultrahigh Carrier Mobility, and Slanted Dirac Cones. *Phys. Rev. B* **2018**, *98*, 085437.

(9) Qin, D.; Yan, P.; Ding, G.; Ge, X.; Song, H.; Gao, G. Monolayer PdSe2: A Promising Two-Dimensional Thermoelectric Material. *Sci. Rep.* **2018**, *8*, 2764.

(10) Yuan, J.-H.; Song, Y.-Q.; Chen, Q.; Xue, K.-H.; Miao, X.-S. Single-Layer Planar Penta-X2N4 (X = Ni, Pd and Pt) as Direct-Bandgap Semiconductors from First Principle Calculations. *Appl. Surf. Sci.* **2019**, *469*, 456–462.

(11) Liu, Z.; Wang, H.; Sun, J.; Sun, R.; Wang, Z. F.; Yang, J. Penta-Pt 2 N 4 : An Ideal Two-Dimensional Material for Nanoelectronics. *Nanoscale* **2018**, *10*, 16169–16177.

(12) Li, J.; Fan, X.; Wei, Y.; Liu, H.; Li, S.; Zhao, P.; Chen, G. Half-Metallicity and Ferromagnetism in Penta-AlN2 Nanostructure. *Sci. Rep.* **2016**, *6*, 1–10.

(13) Lei, W.; Wang, W.; Ming, X.; Zhang, S.; Tang, G.; Zheng, X.; Li, H.; Autieri, C. Structural Transition, Metallization, and Superconductivity in Quasi-Two-Dimensional Layered PdS2 under Compression. *Phys. Rev. B* **2020**, *101*, 205149.

(14) Ma, Y.; Kou, L.; Li, X.; Dai, Y.; Heine, T. Room Temperature Quantum Spin Hall States in Two-Dimensional Crystals Composed of Pentagonal Rings and Their Quantum Wells. *NPG Asia Mater.* **2016**, *8*, e264–e264.

(15) Jing, Y.; Ma, Y.; Wang, Y.; Li, Y.; Heine, T. Ultrathin Layers of PdPX (X=S, Se): Two Dimensional Semiconductors for Photocatalytic Water Splitting. *Chem. - A Eur. J.* **2017**, *23*, 13612–13616.

(16) Qu, Y.; Kwok, C. T.; Shao, Y.; Shi, X.; Kawazoe, Y.; Pan, H. Pentagonal Transition-Metal (Group X) Chalcogenide Monolayers: Intrinsic Semiconductors for Photocatalysis. *Int. J. Hydrogen Energy* **2021**, *46*, 9371–9379.

(17) Konar, S.; Nylén, J.; Svensson, G.; Bernin, D.; Edén, M.; Ruschewitz, U.; Häussermann, U. The Many Phases of CaC2. *J. Solid State Chem.* **2016**, *239*, 204–213.

(18) Bahr, H. A.; Bahr, T. Die Kohlenoxyd-Spaltung an Nickel. *Berichte der Dtsch. Chem. Gesellschaft (A B Ser.* **1928**, *61*, 2177–2183.

(19) Zwell, L.; Fasiska, E. J.; Nakada, Y.; Keh, A. S. Dilation of Nickel Lattice by Dissolved Carbon. *Trans. Mettalurgical Soc. AIME* **1968**, *242*, 765.

(20) Bykov, M.; Yusenko, K. V.; Bykova, E.; Pakhomova, A.; Kraus, W.; Dubrovinskaia, N.; Dubrovinsky, L. Synthesis of Arsenopyrite-Type Rhodium Pernitride RhN2 from a Single-Source Azide Precursor. *Eur. J. Inorg. Chem.* **2019**, *2019*, 3667–3671.

(21) Niwa, K.; Terabe, T.; Suzuki, K.; Shirako, Y.; Hasegawa, M. High-Pressure Stability and Ambient Metastability of Marcasite-Type Rhodium Pernitride. *J. Appl. Phys.* **2016**, *119*, 065901.

(22) Niwa, K.; Yamamoto, T.; Sasaki, T.; Hasegawa, M. High-Pressure Synthesis, Crystal Growth, and Compression Behavior of Hexagonal CrN_2 Having One-Dimensionally Aligned Nitrogen Dimer. *Phys. Rev. Mater.* **2019**, *3*, 053601.

(23) Niwa, K.; Terabe, T.; Kato, D.; Takayama, S.; Kato, M.; Soda, K.; Hasegawa, M. Highly Coordinated Iron and Cobalt Nitrides Synthesized at High Pressures and High Temperatures. *Inorg. Chem.* **2017**, *56*, 6410–6418.

(24) Niwa, K.; Ogasawara, H.; Hasegawa, M. Pyrite Form of Group-14 Element Pernitrides Synthesized at High Pressure and High Temperature. *Dalt. Trans.* **2017**, *46*, 9750–9754.

(25) Bykov, M.; Tasca, K. R.; Batyrev, I. G.; Smith, D.; Glazyrin, K.; Chariton, S.; Mahmood, M.; Goncharov, A. F. Dinitrogen as a Universal Electron Acceptor in Solid-State Chemistry: An Example of Uncommon Metallic Compounds Na3(N2)4 and NaN2. *Inorg. Chem.* **2020**, *59*, 14819–14826.

(26) Bykov, M.; Chariton, S.; Fei, H.; Fedotenko, T.; Aprilis, G.; Ponomareva, A. V.; Tasnádi, F.; Abrikosov, I. A.; Merle, B.; Feldner, P.; Vogel, S.; Schnick, W.; Prakapenka, V. B.; Greenberg, E.; Hanfland, M.; Pakhomova, A.; Liermann, H.-P.; Katsura, T.; Dubrovinskaia, N.; Dubrovinsky, L. High-Pressure Synthesis of Ultraincompressible Hard Rhenium Nitride Pernitride $Re_2(N_2)(N)_2$ Stable at Ambient Conditions. *Nat. Commun.* **2019**, *10*, 2994.

(27) Binns, J.; Donnelly, M.-E.; Peña-Alvarez, M.; Wang, M.; Gregoryanz, E.; Hermann, A.; Dalladay-Simpson, P.; Howie, R. T. Direct Reaction between Copper and Nitrogen at High Pressures and Temperatures. *J. Phys. Chem. Lett.* **2019**, *10*, 1109–1114.

(28) Crowhurst, J. C.; Goncharov, A. F.; Sadigh, B.; Evans, C. L.; Morral, P. G.; Ferreira, J. L.; Nelson, A. J. Synthesis and Characterization of the Nitrides of Platinum and Iridium. *Science.* **2006**, *311*, 1275–1278.

(29) Crowhurst, J. C.; Goncharov, A. F.; Sadigh, B.; Zaug, J. M.; Aberg, D.; Meng, Y.; Prakapenka, V. B. Synthesis and Characterization of Nitrides of Iridium and Palladium. *J. Mater. Res.* **2008**, *23*, 1–5.

(30) Niwa, K.; Fukui, R.; Terabe, T.; Kawada, T.; Kato, D.; Sasaki, T.; Soda, K.; Hasegawa, M. High-Pressure Synthesis and Phase Stability of Nickel Pernitride. *Eur. J. Inorg. Chem.* **2019**, *2019*, 3753–3757.

(31) Bykov, M.; Fedotenko, T.; Chariton, S.; Laniel, D.; Glazyrin, K.; Hanfland, M.; Smith, J. S.; Prakapenka, V. B.; Mahmood, M. F.; Goncharov, A. F.; Ponomareva, A. V.; Tasnádi, F.; Abrikosov, A. I.; Bin Masood, T.; Hotz, I.; Rudenko, A. N.; Katsnelson, M. I.; Dubrovinskaia, N.; Dubrovinsky, L.; Abrikosov, I. A. High-Pressure Synthesis of Dirac Materials: Layered van der Waals Bonded BeN4 Polymorph. *Phys. Rev. Lett.* **2021**, *126*, 175501.

(32) Åberg, D.; Erhart, P.; Crowhurst, J.; Zaug, J. M.; Goncharov, A. F.; Sadigh, B. Pressure-Induced Phase Transition in the Electronic Structure of Palladium Nitride. *Phys. Rev. B* **2010**, *82*, 104116.

(33) Schneider, S. B.; Frankovsky, R.; Schnick, W. Synthesis of Alkaline Earth Diazenides $M_{AE}N_2$ (M_{AE} = Ca, Sr, Ba) by

Controlled Thermal Decomposition of Azides under High Pressure. *Inorg. Chem.* **2012**, *51*, 2366–2373.

(34) Rahm, M.; Cammi, R.; Ashcroft, N. W.; Hoffmann, R. Squeezing All Elements in the Periodic Table: Electron Configuration and Electronegativity of the Atoms under Compression. *J. Am. Chem. Soc.* **2019**, *141*, 10253–10271.

(35) Bykov, M.; Bykova, E.; Aprilis, G.; Glazyrin, K.; Koemets, E.; Chuvashova, I.; Kupenko, I.; McCammon, C.; Mezouar, M.; Prakapenka, V.; Liermann, H.-P.; Tasnádi, F.; Ponomareva, A. V.; Abrikosov, I. A.; Dubrovinskaia, N.; Dubrovinsky, L. Fe-N System at High Pressure Reveals a Compound Featuring Polymeric Nitrogen Chains. *Nat. Commun.* **2018**, *9*, 2756.

(36) Schneider, S. B.; Frankovsky, R.; Schnick, W. Synthesis of Alkaline Earth Diazenides MAEN2 (MAE = Ca, Sr, Ba) by Controlled Thermal Decomposition of Azides under High Pressure. *Inorg. Chem.* **2012**, *51*, 2366–2373.

(37) Deng, Y.; Huang, L.; Dong, X.; Wang, L.; Ok, K. M.; Zeng, H.; Lin, Z.; Zou, G. K2Sb(P2O7)F: Cairo Pentagonal Layer with Bifunctional Genes Reveal Optical Performance. *Angew. Chemie Int. Ed.* **2020**, *59*, 21151–21156.

(38) Wang, S.; Yu, X.; Lin, Z.; Zhang, R.; He, D.; Qin, J.; Zhu, J.; Han, J.; Wang, L.; Mao, H.; Zhang, J.; Zhao, Y. Synthesis, Crystal Structure, and Elastic Properties of Novel Tungsten Nitrides. *Chem. Mater.* **2012**, *24*, 3023–3028.

(39) Bosak, A.; Krisch, M.; Mohr, M.; Maultzsch, J.; Thomsen, C. Elasticity of Single-Crystalline Graphite: Inelastic X-Ray Scattering Study. *Phys. Rev. B* **2007**, *75*, 153408.

(40) Bosak, A.; Serrano, J.; Krisch, M.; Watanabe, K.; Taniguchi, T.; Kanda, H. Elasticity of Hexagonal Boron Nitride: Inelastic X-Ray Scattering Measurements. *Phys. Rev. B* **2006**, *73*, 041402.

(41) Feldman, J. L. Elastic Constants of 2H-MoS2 and 2H-NbSe2 Extracted from Measured Dispersion Curves and Linear Compressibilities. *J. Phys. Chem. Solids* **1976**, *37*, 1141–1144.

(42) Filippatos, P. P.; Hadi, M. A.; Christopoulos, S.-R. G.; Kordatos, A.; Kelaidis, N.; Fitzpatrick, M. E.; Vasilopoulou, M.; Chroneos, A. 312 MAX Phases: Elastic Properties and Lithiation. *Materials (Basel).* **2019**, *12*, 4098.

(43) Zabel, H. Phonons in Layered Compounds. *J. Phys. Condens. Matter* **2001**, *13*, 7679–7690.

(44) Wang, W.; Dai, S.; Li, X.; Yang, J.; Srolovitz, D. J.; Zheng, Q. Measurement of the Cleavage Energy of Graphite. *Nat. Commun.* **2015**, *6*, 7853.

(45) Zhao, K.; Li, X.; Wang, S.; Wang, Q. 2D Planar Penta-MN2 (M = Pd, Pt) Sheets Identified through Structure Search. *Phys. Chem. Chem. Phys.* **2019**, *21*, 246–251.

(46) Zhao, K.; Guo, Y.; Wang, Q. Contact Properties of a VdW Heterostructure Composed of Penta-Graphene and Penta-BN 2 Sheets . *J. Appl. Phys.* **2018**, *124*, 165103.

(47) Pigott, J. S.; Ditmer, D. A.; Fischer, R. A.; Reaman, D. M.; Hrubiak, R.; Meng, Y.; Davis, R. J.; Panero, W. R. High-Pressure, High-Temperature Equations of State Using Nanofabricated Controlled-Geometry Ni/SiO2/Ni Double Hot-Plate Samples. *Geophys. Res. Lett.* **2015**, *42*, 10239–10247.

(48) Mao, H. K.; Xu, J.; Bell, P. M. Calibration of the Ruby Pressure Gauge to 800 Kbar under Quasi-Hydrostatic Conditions. *J. Geophys. Res.* **1986**, *91*, 4673–4676.

(49) Prescher, C.; Prakapenka, V. B. DIOPTAS: A Program for Reduction of Two-Dimensional X-Ray Diffraction Data and Data Exploration. *High Press. Res.* **2015**, *35*, 223–230.

(50) Sheldrick, G. M. SHELXT – Integrated Space-Group and Crystal-Structure Determination. *Acta Crystallogr. Sect. A Found. Adv.* **2015**, *71*, 3–8.

(51) Petricek, V.; Dusek, M.; Palatinus, L. Crystallographic Computing System JANA2006: General Features. *Zeitschrift für Krist.* **2014**, *229*, 345–352.

(52) Dolomanov, O. V.; Bourhis, L. J.; Gildea, R. J.; Howard, J. A. K.; Puschmann, H. OLEX2: A Complete Structure Solution, Refinement and Analysis Program. *J. Appl. Crystallogr.* **2009**, *42*, 339–341.

(53) Holtgrewe, N.; Greenberg, E.; Prescher, C.; Prakapenka, V. B.; Goncharov, A. F. Advanced Integrated Optical Spectroscopy System for Diamond Anvil Cell Studies at GSECARS. *High Press. Res.* **2019**, *39*, 457–470.

(54) Blöchl, P. E. Projector Augmented-Wave Method. *Phys. Rev. B* **1994**, *50*, 17953–17979.

(55) Kresse, G.; Furthmüller, J. Efficiency of *ab Initio* Total Energy Calculations for Metals and Semiconductors Using a Plane-Wave Basis Set. *Comput. Mater. Sci.* **1996**, *6*, 15–50.

(56) Kresse, G.; Furthmüller, J. Efficient Iterative Schemes for *ab Initio* Total-Energy Calculations Using a Plane-Wave Basis Set. *Phys. Rev. B* **1996**, *54*, 11169–11186.

(57) Kresse, G.; Joubert, D. From Ultrasoft Pseudopotentials to the Projector Augmented-Wave Method. *Phys. Rev. B* **1999**, *59*, 1758–1775.

(58) Klimeš, J.; Bowler, D. R.; Michaelides, A. van der Waals Density Functionals Applied to Solids. *Phys. Rev. B* **2011**, *83*, 195131.

(59) Togo, A.; Tanaka, I. First Principles Phonon Calculations in Materials Science. *Scr. Mater.* **2015**, *108*, 1–5.

(60) Bader, R. F. W. *Atoms in Molecules: A Quantum Theory*; Clarendon Press: Oxford, 1994.

(61) Sanville, E.; Kenny, S. D.; Smith, R.; Henkelman, G. Improved Grid-Based Algorithm for Bader Charge Allocation. *J. Comput. Chem.* **2007**, *28*, 899–908.

(62) Nye, J. F. *Physical Properties of Crystals*; Clarendon Press: Oxford, 1985.

(63) Heyd, J.; Scuseria, G. E.; Ernzerhof, M. Erratum: "Hybrid Functionals Based on a Screened Coulomb Potential" [J. Chem. Phys. 118, 8207 (2003)]. *J. Chem. Phys.* **2006**, *124*, 219906.

(64) Heyd, J.; Scuseria, G. E.; Ernzerhof, M. Hybrid Functionals Based on a Screened Coulomb Potential. *J. Chem. Phys.* **2003**, *118*, 8207–8215.

(65) Perdew, J. P.; Burke, K.; Ernzerhof, M. Generalized Gradient Approximation Made Simple. *Phys. Rev. Lett.* **1996**, *77*, 3865–3868.